JGR Oceans

RESEARCH ARTICLE
10.1029/2021JC018387

Key Points:

- Air sea fluxes of noble gases initially increase as wind speed increases from 20 to 35 m s^{-1} but then level off at higher speeds
- Steady state saturation anomalies are more strongly correlated with bubble volume and significant wave height than with wind speed
- Invasion fluxes are larger in magnitude than evasion fluxes under similar conditions

Supporting Information:

Supporting Information may be found in the online version of this article.

Correspondence to:

R. H. R. Stanley,
rachel.stanley@wellesley.edu

Citation:

Stanley, R. H. R., Kinjo, L., Smith, A. W., Aldrett, D., Alt, H., Kopp, E., et al. (2022). Gas fluxes and steady state saturation anomalies at very high wind speeds. *Journal of Geophysical Research: Oceans*, *127*, e2021JC018387. https://doi.org/10.1029/2021JC018387

Received 24 DEC 2021
Accepted 25 JUL 2022

Gas Fluxes and Steady State Saturation Anomalies at Very High Wind Speeds

Rachel H. R. Stanley[1], Lumi Kinjo[1], Andrew W. Smith[2], Danielle Aldrett[1], Helene Alt[1], Emily Kopp[1], Callan Krevanko[1], Kevin Cahill[3], and Brian K. Haus[2]

[1]Wellesley College, Wellesley, MA, USA, [2]Rosenstiel School of Marine and Atmospheric Science, University of Miami, Miami, FL, USA, [3]Woods Hole Oceanographic Institution, Woods Hole, MA, USA

Abstract Gas exchange at high wind speeds is not well understood—few studies have been conducted at wind speeds above 20 ms^{-1} and significant disagreement exists between gas exchange models at high wind speeds. In this study, noble gases (He, Ne, Ar, Kr, and Xe) were measured in 35 experiments in the SUSTAIN wind-wave tank where the wind speeds ranged from 20 to 50 m s^{-1} and mechanical waves were generated as monochromatic or with a short-crested JONSWAP frequency spectrum. Bubble size spectra were determined using shadowgraph imagery and wave statistics were measured using a wave wire array. The steady state saturation anomalies and gas fluxes initially increased as wind speeds increased but then leveled off, similar to prior studies of heat and momentum flux coefficients. Noble gas fluxes and steady state saturation anomalies are correlated most strongly with bubble volumes for the less soluble noble gases and with wind speed and wave Reynolds number for the more soluble noble gases. In the JONSWAP experiments, significant wave height was the most important predictor for gas steady state saturation anomalies with correlation coefficients of greater than 0.92 for He, Ne, and Ar ($P < 0.05$). Furthermore, invasion fluxes were larger than evasion fluxes when other conditions were similar. Taken together, these lab-based experiments suggest more attention should be paid to parameterizations based on wave characteristics and bubbles and that current wind-speed based gas exchange parameterizations should not be applied to conditions with very high wind speeds.

Plain Language Summary Gases, such as carbon dioxide, are transferred between the atmosphere and the ocean. Understanding how much gas goes back and forth and how we, as humans, can best predict that, is really important for accurately predicting the effects of climate change. Gas transfer is hard to measure directly so often scientists make estimates, also known as parameterizations, of gas transfer based on the easy to measure variable wind speed. These parameterizations are typically based on data from wind speeds of less than 25 m s^{-1} since it is hard to sample the ocean in high wind conditions. Current parameterizations expect that at higher wind speeds, the gas transfer will increase dramatically, increasing as either the square or the cube of the wind speed. In this study, we conducted experiments at wind speeds up to 50 m s^{-1} (category III hurricane) in a controlled wind-wave tank in order to directly study gas exchange at very high wind speeds. We found a surprising behavior—above a certain wind speed, the gas transfer stopped changing, even as wind speed increased more. We also found that using wave characteristics and bubble volume enabled better prediction of gas transfer than just using wind speed.

1. Introduction

Gas exchange is a key part of the biogeochemical cycle of many climatically important gases, such as CO_2, N_2O, and DMS, as well as of O_2 which is increasingly being used to quantify rates of biological production and CO_2 uptake through the biological pump (e.g., Alkire et al., 2014; Emerson, 2014; Hamme et al., 2012; Johnson & Bif, 2021; Juranek et al., 2012; Nicholson et al., 2015; Palevsky et al., 2016; Plant et al., 2016; Stanley et al., 2015). Much progress has been made in developing air-sea gas exchange parameterizations that give accurate estimates of fluxes for multiple gases in a variety of wind conditions (D'Asaro & McNeil, 2007; Ho et al., 2011; McNeil & D'Asaro, 2007; Sweeney et al., 2007; Vagle et al., 2010; Wanninkhof et al., 2009; Wrobel & Piskozub, 2016). Nonetheless, these parameterizations still differ from each other widely at high wind speeds. The gas flux due to bubbles is explicitly represented in some parameterizations (Asher et al., 1996; Blomquist et al., 2017; Fairall et al., 2011; Goddijn-Murphy et al., 2016; Liang et al., 2013; Nicholson et al., 2011; Stanley, Jenkins, et al., 2009; Woolf et al., 2007; Zhang, 2012). However, this bubble contribution, which becomes increasingly important as wind speed increases, is not explicitly represented in many commonly used air-sea gas

exchange parameterizations (Ho et al., 2011; Nightingale et al., 2000; Wanninkhof, 1992, 2014) leading to errors at high wind speeds (Liang et al., 2020).

Bubble fluxes represent a larger contribution to the flux of less soluble gases, such as the noble gases used in this experiment or for O_2, than for the more soluble greenhouse gases such as CO_2, CH_4, and N_2O. However, bubble fluxes likely also contribute significantly to overall gas fluxes of CO_2—a combined data and modeling study showed a significant suppression of CO_2 outgassing during a hurricane because of the invasion of CO_2 from bubbles during the high winds of the storm (Liang et al., 2020). At more moderate wind speeds, such as those between ∼10 and 30 m s^{-1}, the discrepancy between CO_2 and DMS in eddy covariance experiments (Bell et al., 2017; Blomquist et al., 2017; Zavarsky et al., 2018) is often attributed to bubble fluxes being important for CO_2 but not DMS. Recent studies suggest that 18%–40% of the air-sea CO_2 flux overall is mediated through bubbles (Gu et al., 2021; Reichil & Deike, 2020). Thus, a better understanding of bubble fluxes is crucial in order to accurately predict CO_2 fluxes at high wind speeds as well as for calculating gas fluxes of less soluble gases such as O_2 and the noble gases. Furthermore, although research has shown that air-sea flux coefficients of momentum and heat level off at very high wind speeds such as $U_{10} > 35$ m s^{-1} (Donelan et al., 2004; Haus et al., 2010; Jarosz et al., 2007; Takagaki et al., 2016), very few studies exist of air-sea gas exchange at high wind speeds to see if this leveling off occurs with gas exchange as well.

Most gas exchange parameterizations parameterize the flux as a function of wind speed at 10 m above the air-sea interface (U_{10}), with wind speed being a proxy for the fundamental turbulent dynamics that are likely truly controlling gas exchange. Some studies have found stronger relationships between gas fluxes and other parameters such as the turbulent kinetic energy (Zappa et al., 2007), wave Reynolds number (Brumer et al., 2017), or sea state including wave statistics (Deike & Melville, 2018; Li et al., 2021; Reichil & Deike, 2020). More research is needed into which parameters are most effective for inclusion in gas exchange parameterizations suitable for high wind environments.

Air-sea gas exchange fluxes are measured with a multitude of techniques, with the most common being the eddy covariance method (e.g., Bell et al., 2017; Blomquist et al., 2012; Huebert et al., 2004; McGillis et al., 2004) or the dual tracer release method (Ho et al., 2006, 2011). A third technique, noble gas mass balances, has been used to study gas exchange as well (Hamme & Emerson, 2006; Nicholson et al., 2011; Spitzer & Jenkins, 1989; Stanley et al., 2006, Stanley, Jenkins, et al., 2009). The noble gas mass balance method requires minimal manipulation of the water (unlike dual tracers), can be used to study invasion or evasion of gases, enables gas fluxes to be determined on longer spatiotemporal scales than eddy covariance, and allows quantification of both diffusive and bubble mediated gas transfer (e.g., Stanley, Jenkins, et al., 2009). The noble gases helium (He), neon (Ne), argon (Ar), krypton (Kr), and xenon (Xe) are biologically and chemically inert, and thus gas exchange is the primary physical process responsible for changes in the concentrations of these gases. Additionally, the solubility of the noble gases differs by approximately a factor of 5 (Hamme & Emerson, 2004; Jenkins et al., 2019) and the diffusivity by a factor of 10 (Jahne et al., 1987) allowing the gases to be used simultaneously as tracers for both bubble-mediated and diffusion gas exchange; the less soluble gases respond more strongly to bubble fluxes compared to the more soluble ones. The solubility of the noble gases is dependent on temperature, especially for the more soluble gases (Jenkins et al., 2019), and thus the water concentrations of the gases depart from equilibrium when the water temperature changes more quickly than the gas flux can modulate. The recent development of a field portable gas equilibration mass spectrometer (GEMS) (Manning et al., 2016) enables continuous measurement of a suite of noble gases (Ne, Ar, Kr, and Xe) with time resolution of 2–6 min. In this study, multiple measurements of the noble gases were used in short (∼1 hr) experiments at a range of wind speeds (20–50 m s^{-1}) in order to investigate gas exchange at high wind speeds.

Very few studies investigate air-sea gas exchange at high wind speeds (>25 m s^{-1}) in the field (D'Asaro & McNeil, 2007; Liang et al., 2020; McNeil & D'Asaro, 2007) due to safety and technological challenges of sampling during hurricane force winds. Even though wind speeds greater than 25 m s^{-1} do not occur globally often (Figure S1 in Supporting Information S1, Ricciardulli & Wentz, 2016), the expected high fluxes associated with such wind speeds (Gu et al., 2021) and the predicted increase in frequency of high wind conditions (Young & Ribal, 2019; I. R. Young et al., 2011) make it important to study gas exchange at high wind speeds. Most experiments at high wind speeds have been done in wind-wave tanks (Krall & Jaehne, 2014; Krall et al., 2019; Mesarchaki et al., 2015), controlled environments where wind is produced by large fans and waves are produced by wave paddles. In this study, experiments to determine the fluxes and the equilibrium steady state saturations

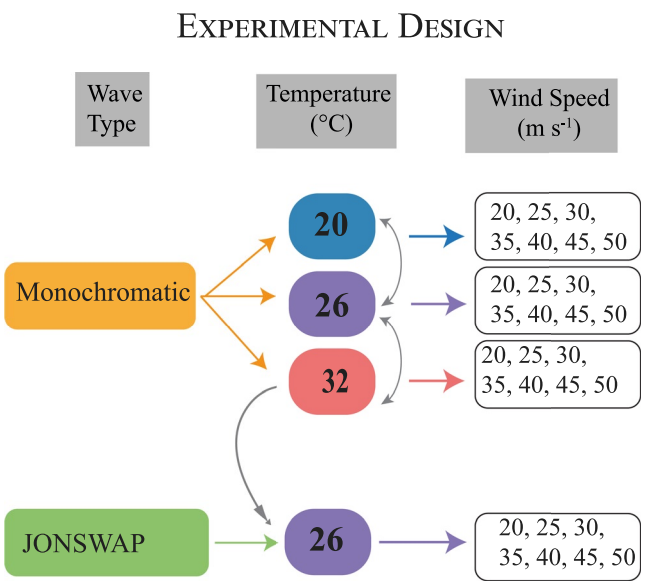

Figure 1. The experimental design consisted of experiments with two different wave types, three water temperatures for the monochromatic wave type but only one temperature for the JONSWAP waves, and seven wind speeds for each wave type/temperature combination. Additionally, experiments were performed (gray arrows) where the water temperature was manipulated immediately prior to the experiment in order to intentionally make the gases supersaturated (when warmed) or undersaturated (when cooled). Those invasion/evasion experiments were performed only with wind speed of 35 m s^{-1}. An exact listing of conditions for every experiment is in Table S1 of Supporting Information S1.

of the noble gases at very high wind speeds (U_{10} from 20 to 50 m s^{-1}, a category 3 hurricane) were performed at the SUrge STructure Atmosphere INteraction (SUSTAIN) Facility, a 23 × 6 × 2 m clear wind-wave tank at the University of Miami (Laxague et al., 2017; Savelyev et al., 2020). A shadowgraph recorded bubble images and a wave wire array was used to quantify wave statistics (Smith et al., 2022). Thus, physical parameters beyond simply wind speed can be related to gas fluxes at very high wind speeds in a controlled system. While wind-wave tanks do not completely mimic reality and thus caution needs to be observed when applying conclusions from tanks to the open ocean, wind wave tanks offer an invaluable opportunity to examine gas transfer in physical conditions that are not easily observable in the field.

2. Materials and Methods

2.1. Experimental Design and the SUSTAIN Wind-Wave Tank

Experiments were performed at the SUrge STructure Atmosphere INteraction (SUSTAIN) Facility at the University of Miami (Laxague et al., 2017; Savelyev et al., 2020). The tank was approximately half filled (to a depth of 0.8 m) with filtered seawater from the adjacent Biscayne Bay, with a salinity of 33.7 psu and incoming temperature of 31.4°C. The water in the tank was temperature controlled and experiments were performed at 26, 32, and 20°C. The SUSTAIN tank has a 1,460 horsepower fan which is capable of producing winds up to 65 m s^{-1}. It also has a 12-element programmable directional wave maker which allows for production of longer period, directional waves to be generated at the wind inlet. A series of 35 experiments were performed over 5 days (Table S1 in Supporting Information S1).

Three main variables were changed in a modified factorial design during the experiments: wind speed, water temperature, and wave type (Figure 1). The air temperature in all the experiments was approximately 26°C. Water temperatures in the tank were controlled by a heat exchanger that applied or removed heat from the recirculating water to be 26°C and thus of neutral atmospheric stability, 20°C and thus a convectively stable system, or 32°C and thus a convectively unstable system. However, at the high wind speeds in this study, atmospheric stability may not be a crucial parameter. Nonetheless, the solubilities and diffusivities of the gases change as a function of temperature (e.g., Jahne et al., 1987; Jenkins et al., 2019) and bubble fluxes have been predicted to be temperature dependent (Jeffery et al., 2010; Liang et al., 2011; Woolf et al., 2007). Thus, exploring multiple water temperatures provides data that may be able to be used to help constrain the temperature dependence of bubble fluxes in mechanistic models.

Waves were either monochromatic, being uniformly produced with a frequency of 1 Hz and a wave height of 0.15 m, or they were randomly generated using a JONSWAP spectrum (Hasselman et al., 1973) to more accurately mimic conditions in the open ocean. Given the greater control over wave breaking and the homogeneity of the monochromatic conditions, experiments at all three temperatures were performed with the monochromatic wave type. Experiments with the JONSWAP waves were only performed at 26°C. The fan frequency was changed so that wind speeds varied in 5 m s^{-1} increments between U_{10} = 20 and 50 m s^{-1} (Smith et al., 2022). Wind speed and water temperature conditions for each of the 35 experiments are listed in Table S1 of Supporting Information S1.

Additional experiments were conducted at wind speeds U_{10} = 35 m s^{-1} to intentionally probe the system when the gases were far from equilibrium because of heating or cooling. Given the temperature dependence of gas solubility, when water is cooled with little gas exchange, the gases become undersaturated. When it is warmed, they become supersaturated. Thus, four experiments were conducted where first the temperature of the tank was changed by 6°C with waves of only amplitude 0.05 m and wind speeds of U_{10} = 10 m s^{-1} (these light winds and waves were necessary to keep the tank well-mixed during the cooling/warming): these occurred with the water changing from 32 to 26°C, 26 to 32°C, 20 to 26°C, and 26 to 20°C (gray arrows in Figure 1). Then, an experiment

was started with $U_{10} = 35$ m s^{-1}, with monochromatic waves, allowing the gases to exchange back and approach equilibrium at the new temperature. Additionally, a similar experiment was conducted when the water temperature was first cooled from 32 to 26°C and then the experiment occurred with $U_{10} = 35$ m s^{-1} and with JONSWAP waves. These experiments allowed probing of whether invasion fluxes—when the gases start undersaturated and thus atmospheric gas is entering the ocean—equal evasion fluxes—when the gases start supersaturated and thus gas is leaving the ocean.

2.2. Discrete Noble Gas Samples and Analysis

At the end of every experiment, and at the beginning of approximately half the experiments (the experiments conducted with $U_{10} = 20$, 30, 40, and 50 m s^{-1} and the invasion/evasion experiments), samples for discrete noble gas analysis were collected in copper tubes (Jenkins et al., 2019; Loose et al., 2016). The samples were drawn from the tank through pre-soaked tygon tubing into 0.76 m of 5/8″ diameter copper tubing, bubbles were removed by rapping, and at least 1 L of water was allowed to flow through the tube. Flow was temporarily stopped by clips and then the ends of the copper tube were cold-welded (C. Young & Lupton, 1983), producing two gas-tight samples of ∼45 g each per time-point, though typically only one sample was analyzed. Samples were shipped to the Isotope Geochemistry Facility at WHOI where the gases were first extracted from the sealed copper tube into 30 mL aluminosilicate glass ampoules using an evacuated noble gas extraction line (Jenkins et al., 2019) and then analyzed for He, Ne, Ar, Kr, and Xe on a quadrupole mass spectrometer by first being separated cryogenically and then using ion beam manometry for He, Ne, and Ar, and isotope dilution for Kr and Xe (given the smaller abundances of Kr and Xe, isotope dilution is required for better precision and accuracy) (Jenkins et al., 2019; Stanley, Baschek, et al., 2009). Precision of the system, based on measurements of duplicate samples, is 0.1% for He, Ne, Ar, Kr, and 0.2% for Xe.

Steady state saturation anomalies, Δ, were calculated from the noble gas concentrations from samples collected at the end of each experiment according to the equation

$$\Delta = \left(\frac{C_{\text{meas}}}{C_{\text{sol}}}\right) \times 100$$

where C_{meas} is the measured concentration of the gas in the sample and C_{sol} is the solubility equilibrium value given by Jenkins et al. (2019) for the measured temperature and salinity of the samples.

2.3. Continuous Gas Records

The noble gas ratios and concentrations of the seawater within the SUSTAIN tank were analyzed continuously using the portable Gas Equilibrator Mass Spectrometer (GEMS) for Ne, Ar, Kr, and Xe ratios (Manning et al., 2016) and an Equilibrator Inlet Mass Spectrometer (EIMS) for O_2/Ar ratios (Cassar et al., 2009). For both systems, water was pumped from a level of 28.75 cm above the bottom of the SUSTAIN tank, just down-fetch from the bubble imager (Figure 2) into a 4 L beaker set up on the level right above the tank (a distance of approximately 2 m) using an in situ fountain pump (Smart Pond 500-Gph), a type of pump that leads to less gas distortion than pumps that pull the water from the top. The beaker was temperature-controlled by outflowing water, and then the outflowing water was circulated back into the tank so that the total volume of water in the tank did not change appreciably.

For the GEMS: a microgear pump, equipped with tygon tubing, brought the water from the bucket through a polyester filter bag (14 cm OD, 38 cm long, and 25 μm pore size) and a filter sock (3.8 cm wide, 30 cm long, and 5 μm inner and 100 μm outer pore size) into a Membrana Liqui-Cell Extra-Flow Equilibration cartridge. The headspace in that cartridge was swept through a nafion box and drierite tubing for drying and then through a 0.05 μm capillary to a gettering system constructed of SAES STS-2001 getters at 350°C and at room temperature for removal of active gases, and finally into a Hiden RGA HAL 3F Quadrupole Mass Spectrometer (for details, see Manning et al., 2016). Precision of the gases, based on laboratory experiments of equilibrated water, conducted immediately before the work at SUSTAIN, suggest that the ratios of noble gases are quantified with precisions better than 0.5% for Ne/Xe and Ar/Kr, and better than 0.8% for Ne/Ar, Ar/Kr, and Ar/Xe. The e-folding equilibration time of the cartridge is several minutes, with ratios being measured every 60 s. Thus, this method, though powerful, may average over the first few minutes of intense gas exchange.

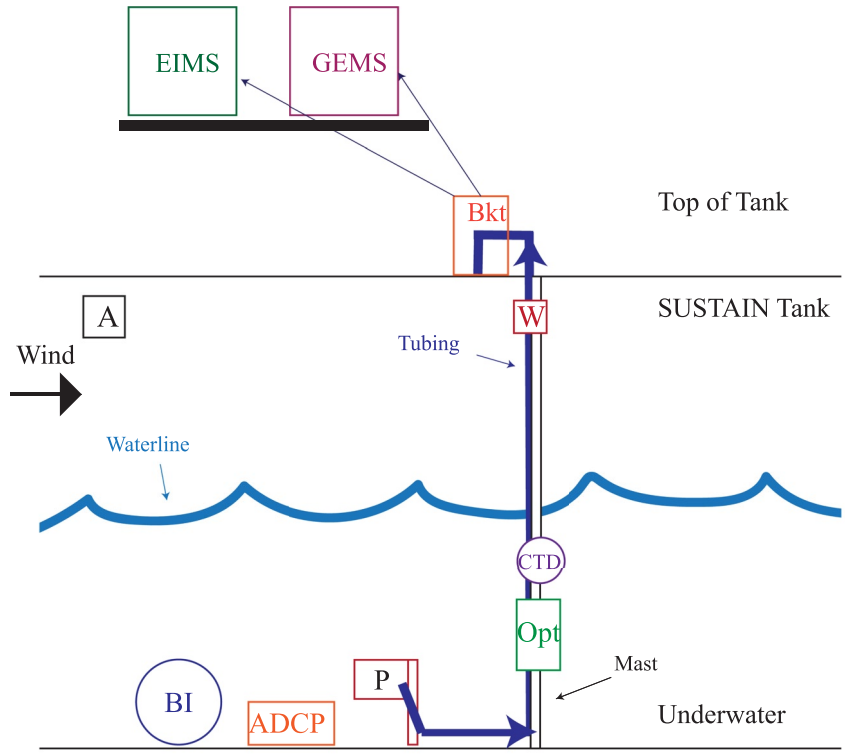

Figure 2. Schematic of instrumentation inside a cross-section view of the SUSTAIN tank, including the area above the tank. Underwater, a bubble imager (BI) was most upstream. It was followed by an ADCP and a water pump (P). Tubing from the water pump was affixed to a mast that provided support for the tubing to be carried above the tank where it entered a bucket (BKT). Microgear pumps were used to carry water from the bucket to the equilibration cartridges for a Gas Equilibrator Mass Spectrometer (GEMS) for measurement of noble gas ratios and for an Equilibrator Inlet Mass Spectrometer (EIMS) for measurement of O_2/Ar. Also affixed to the mast underwater was an optode (Opt) and a CTD. One of the three wave wires (W) in the wave wire array ran parallel to the mast. The other two wave wires were downwind and off-center (not shown in this schematic). A sonic anemometer (A) was upstream of the instrumentation, and was also off-center so as not to block the wind flow in the main instrumentation section. Elsewhere in the tank there were additional instrumentation; see text for details.

For the EIMS: a second Liqui-Cel Extra-Flow Equilibration cartridge, complete with its own filters, gear pump, and air circulation loop (all similar to the ones for the GEMS), was set up and gas from that cartridge was fed into a Pfeiffer PrismaPlus Quadrupole Mass Spectrometer for analysis of O_2/Ar. Notably, this second system was similar to the first but it did not have getters, allowing analysis of O_2 (which is removed by the getters). Measurements were collected every 15 s and e-folding equilibration time of the cartridge is similarly several minutes.

Both the GEMS and the EIMS contained Vici valves that allowed switching between the capillary connected to the cartridges that were sampling the gas content of water in the SUSTAIN tank and the capillaries that were measuring laboratory air which was used for standardization of gas ratios since the gas content of oxygen and noble gases in air is constant and well-known. Before and after each experiment, the GEMS and the EIMS sampled laboratory air. These frequent calibrations were necessary because the humidity and temperature of the SUSTAIN lab building increased during the day as hot Miami air was blown through the system. Frequent air calibrations allowed us to correct for these humidity and temperature effects on the mass spectrometers. Additionally, experiments were conducted where the GEMS sampled air that was within the SUSTAIN tank itself to confirm that the SUSTAIN tank air (i.e., air directly overlying the water) was the same as the general laboratory air. However, due to the risk of salt spray getting into the air capillary and subsequently into the mass spectrometer, most of the air calibrations were performed using laboratory air.

Ratios of gases in either the GEMS (e.g., Ne/Xe, Ar/Kr, or any combination thereof) or the EIMS (O_2/Ar) were calculated according to Manning et al., 2016 with the gas ratios in air interpolated between the start and end of

each experiment (roughly 1 hr interval) and then the measured gas ratios in water related to the air ratios according to:

$$\Delta\left(\frac{\mathrm{Ne}}{\mathrm{Xe}}\right)=\left[\frac{\left(\frac{\mathrm{Ne}}{\mathrm{Xe}}\right)_{hs}}{\left(\frac{\mathrm{Ne}}{\mathrm{Xe}}\right)_{\mathrm{air}}}-1\right]\times 100$$

where *hs* refers to the gas ratio in the headspace of the cartridge and air refers to the gas ratio as measured in laboratory air.

Oxygen concentrations were measured every 5 s using an Anderra optode deployed directly in the tank, affixed 35 cm above the tank bottom to the main mast from which the water was pumped. The optode was calibrated with oxygen samples measured using the Winkler method by F. Millero's laboratory at the University of Miami.

The GEMS furnishes ratios of noble gases in seawater. These ratios are informative, since for example, bubbles impact the saturation anomaly of Ne much more than they affect Xe due to Ne's lower solubility and thus the Ne/Xe ratio can be used as a diagnostic for the influence of bubble processes. However, for flux calculations, concentrations of the gases are necessary. Thus, we calculated noble gas concentrations from the continuous GEMS record by combining the optode O_2 concentrations, the EIMS O_2/Ar ratios, and the GEMS Ne/Ar, Kr/Ar, and Xe/Ar ratios, according to the equation (given for Xe but analogous equations can be written for other gases):

$$[\mathrm{Xe}]=\mathrm{O_{2optode}}\times\left(\frac{\mathrm{Ar}}{\mathrm{O_2}}\right)_{\mathrm{EIMS}}\times\left(\frac{\mathrm{Xe}}{\mathrm{Ar}}\right)_{\mathrm{GEMS}}$$

where Ar/O_2 is the air-calibrated ratio of ion currents of Ar and O_2 as measured in the headspace by the EIMS and Xe/Ar is air-calibrated ratio of the ion currents of Xe and Ar as measured in the headspace by the GEMS.

We then compared these calculated concentrations, which are obtained at one-minute time resolution, to the concentrations from the 53 discrete samples of the noble gases. In particular, by matching the time of the continuous data, we calculated a correction factor for each gas and each water temperature since the GEMS equilibration success is dependent on temperature. At 26°C, the correction factors varied from 1.004 to 1.01 with Ne having the smallest and Ar the largest. At 20°C, the correction factors varied from 0.950 to 0.956 with Kr having the smallest and Xe the largest. At 32°C, the correction factors varied from 0.97 to 1.02 with Xe having the smallest and Ne the largest.

Fluxes of noble gases were calculated as the change in concentration of a gas divided by time over which that change occurred. In particular, a linear curve was fit to the data from 2 to 12 min of the experiment (the time when the gas concentrations were most rapidly changing) and the slope of that line is used as the flux. In some cases, the Ne concentrations stopped changing more quickly (likely because the increased diffusivity of Ne makes it reach steady state more quickly) and thus only 6–8 min were used for the linear fitting. Errors were calculated as the error associated with the slope of the type 1 regression. These errors include the error in the individual data points since noise in the data leads to a noisier slope. Errors from the Winkler, optode, and EIMS O_2/Ar are all significantly smaller (0.2%) compared to the error from the curve fitting (~10%). Additionally, "Quasi-instantaneous" fluxes were calculated as the change in gas concentration divided by the smallest time increment measured, that is, 1-min. Fluxes calculated as the mean of the quasi-instantaneous fluxes agreed well with the linear fitting approach.

2.4. Bubble Imaging

An in-situ bubble imaging shadowgraph system (Ozgokmen et al., 2018) was used to quantify the number and size distribution of bubbles in a control volume of 3.524×10^{-4} m^3 which was comprised of a 0.0685×0.0515 m field of view at 5 s intervals during each of the experiments (Smith et al., 2022). Paired Fresnel lenses collimate a LED Luxeon Rebel royal blue light source (470 nm) in order to reduce the dependency of the observed bubble size to the position of the bubble in the water column. Image processing of the contrast gradients was used to identify bubbles via a Circular Hough transform (Atherton & Kerbyson, 1999) and resulted in the quantification of the number of bubbles in each radius bin between 30.25 and 1512.5 μm and thus allows calculation of void

fraction and bubble size distributions. In order to achieve summary statistics used for comparison with the noble gases, the average void fraction due to bubbles and the average surface area of the bubbles were calculated from each bubble spectrum at every time point within a 10-min window starting at the beginning of each experiment. For further details on the bubble shadowgraph and how bubble distributions were calculated, we direct the reader to Smith et al. (2022). Bubble size distributions and the associated void fractions for the experiments described in this paper are shown in Figure 11 of Smith et al. (2022). Additionally, the bubble images can be accessed at https://www.bco-dmo.org/project/776111.

2.5. Surface Wave Statistics

Water surface elevation and individual wave crest statistics, including wave height, steepness, skewness, and asymmetry, were measured using an array consisting of three 2m long Ocean Sensor Systems WS Type III wave wires. The wave wires were arranged in an equilateral triangle of length 0.283 m for each side. Each wave wire recorded at 20 Hz sampling frequency. The wave wire data were detrended to account for water loss due to spray ejection. Individual wave crests and troughs were identified using zero-crossing and signal peak detection algorithms (Babanin et al., 2007). Directional wave spectra were determined using the Wavelet Directional Method with the Morlet wavelet (Donelan et al., 1996). Water surface elevation spectra were used to calculate significant wave height (H_s) and wave steepness $\delta = (H/2)k = ak$. Details on the statistical wave analysis are given in Smith et al. (2022). Additionally, H_s is combined with wind speed measurements to calculate the wind-wave Reynolds number, Re_{Hw} (Brumer et al., 2017), defined as

$$Re_{Hw} = u_* H_s \nu_w^{-1}$$

where u_* is the frictional velocity and ν_w is the water viscosity.

2.6. Ancillary Data

Temperature and salinity were measured at 4 locations within the tank using in-situ Decagon conductivity-temperature-depth (CTD) sensors. Two of these were placed very near the water pump for the gases at depths of 0.125 and 0.465 m above the bottom of the tank. The other two were placed at the extreme ends of the tank, so 9.81 and 6.31 m upstream and downstream of the water pump, respectively. Currents were measured using two upward-facing Nortek acoustic Doppler current profilers (ADCP). One ADCP was a four beam fast-sampling Vectrino profiler and the other was a three beam 2 MHz Aquadopp HR high resolution full-depth profiler. Turbulence measurements for this analysis were calculated from the Vectrino at 100 Hz sampling resolution, 0.34 m downstream from the water pump. For details on how turbulent kinetic energy (TKE) was calculated from the Vectrino measurements in this study, see Smith et al. (2022).

U_{10} was calculated assuming neutral stability according to

$$U_{10} = U_z + \frac{u_*}{\kappa} \log \frac{10}{z}$$

where U_z is the wind speed at the sonic anemometer height $z = 0.59$ m, u_* is the friction velocity, and κ is the von Karman constant 0.41. Details on the relationship between fan speed and U_{10} are in Smith et al. (2022).

2.7. Correlation Analysis

In order to elucidate connections between physical variables (bubble volume, bubble surface area, H_s, turbulent kinetic energy (TKE), and wind speed) and gas steady state saturation anomalies and fluxes, multilinear correlations were calculated using the gas values as dependent variables and the physical variables as independent variables using the MATLAB function fitlm. Adjusted R^2 values (adjusted to take into account the increase in R^2 simply due to the complexity of the model increasing) and the significance of the correlation (p-value) are determined as part of fitlm. Multilinear correlations were performed with all the data, using temperature and wave type as categorical variables, and also with subsets of the data, such as just the JONSWAP experiments or only the monochromatic experiments at 26°C.

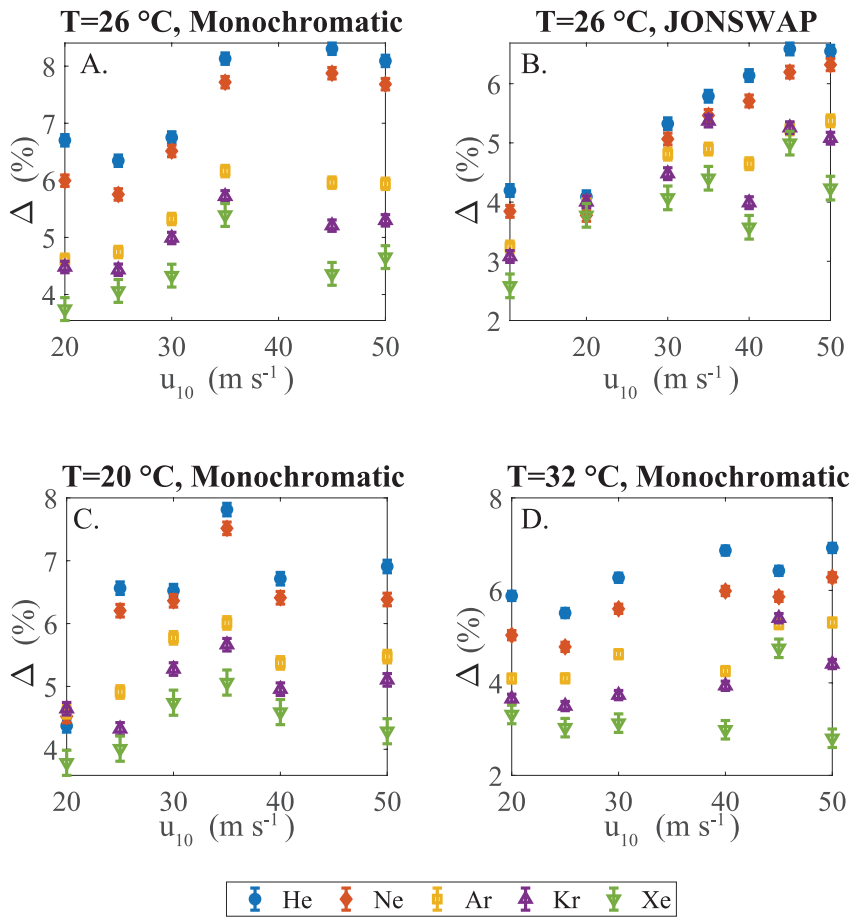

Figure 3. Steady state saturations of the noble gases as measured in discrete copper tube samples collected at the end of each experiment for experiments with: (a) monochromatic waves at 26°C water temperature, (b) JONSWAP waves at 26°C water temperature, (c) monochromatic waves at 20°C water temperature, and (d) monochromatic waves at 32°C water temperatures. Experiments where the temperature of the tank was changed immediately prior to the experiment are not included in this figure. Error bars reflect measurement error. Note that while the steady state saturation anomalies initially increase as wind speed increases, they then level off. Additionally, the less soluble gases such as He and Ne, which are the most sensitive to bubble processes have larger steady state saturation anomalies than more soluble gases such as Kr and Xe.

3. Results and Discussion

3.1. Steady State Saturation Anomalies

The steady state saturation anomalies of the noble gases, determined at the end of each experiment, are plotted as a function of wind speed for the four experimental conditions (monochromatic waves at water temperatures of 20, 26, and 32°C, JONSWAP waves at water temperature of 26°C) (Figure 3). These saturation anomalies reflect steady state conditions (Liang et al., 2013): the quasi-equilibrium state produced by balancing the bubble flux in and the diffusive flux out. Notably, these experiments were carried out at constant temperature with no deliberate manipulation of gas content in the water and thus the main contributor to gas flux is invasion due to bubbles formed at the larger wind speeds, balanced by evasion due to diffusive gas transfer. The lighter, less soluble gases such as He and Ne have larger steady state saturation anomalies than the heavier, more soluble gases such as Kr and Xe because of the increased effect of bubbles on the lower solubility gases. This result has been observed in the real ocean as well (Hamme & Severinghaus, 2007; Stanley, Jenkins, et al., 2009). Additionally, the difference in saturation anomalies between the lighter and heavier gases (e.g., ΔHe-ΔXe) increases as wind speed increases, another expected observation caused by the greater sensitivity of He to bubbles and the larger population of bubbles at higher wind speeds.

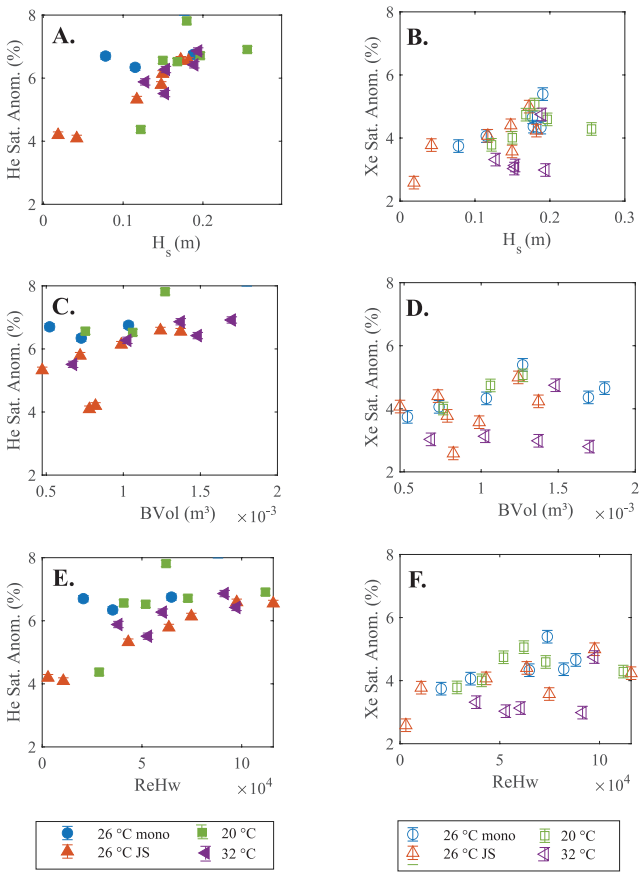

Figure 4. Saturation State Anomalies (Δ) of He (panels a, c, and e) and Xe (panels b, d, and f) plotted versus three variables that explain a large amount of the variance in the data: significant wave height H_s, bubble volume *BVol*, and wave Reynolds Number, Re_{Hw}. Different environmental conditions are plotted in different colors and error bars reflect the measurement error associated with the noble gas data. The He saturation state anomalies are always larger than the Xe ones due to the greater importance of bubbles for the less soluble He. Furthermore, the He saturation state anomalies are more strongly correlated with the physical variables than the Xe saturation anomalies are.

In most cases, the steady state saturation anomalies increase as wind speed increases and then level off—the exact wind speed at which the leveling off occurs differs for the various environmental conditions, likely because wind speed is not a single fundamental characteristic that controls gas transfer. For example, the leveling off occurs at a higher wind speed in the JONSWAP wave cases than in the monochromatic experiments because the steeper monochromatic waves result in more intense wave breaking and subsequently greater air entrainment for a given wind speed. Furthermore, when the steady state saturation anomalies are plotted versus significant wave height (Figures 4a and 4b), the anomalies increase as H_s increases and do not level off, suggesting H_s is a more fundamental control/variable on the anomalies than wind speed is (Deike & Melville, 2018). Note that these experiments were done in a wind-wave tank with a maximum water depth of ~85 cm. Thus, the waves generated by the wave paddles and wind are much smaller in these experiments than the real waves in the ocean. Since even the small waves are a significant predictor of gas flux in this experiment, it suggests that in the ocean, waves might have an even larger impact and be even more important. While the artificial conditions including the shallow depth of the wind-wave tank makes extracting concrete parameters that can be directly used in ocean parameterizations unlikely, the controlled nature of the experiments and the possibility of obtaining very high wind speeds allows these experiments to pinpoint promising areas of future study such as including significant wave height directly in gas exchange parameterizations.

The experiments with JONSWAP waves have the strongest correlations between steady state saturation anomalies and significant wave height (Table 1), likely because the significant wave height varied the most in those experiments—in the monochromatic wave experiments, wave height was fixed by the paddles to be constrained to a relatively narrow range and thus correlations between gases and H_s are weaker. In the JONSWAP case, the Pearson correlation coefficients between H_s and ΔHe is $R^2 = 0.95$ and between H_s and ΔXe is $R^2 = 0.52$. It is not surprising that the lighter gases have stronger correlation coefficients since the lighter gases are less soluble and thus more sensitive to bubble processes. Wave breaking is associated with bubble generation, as well as increased surface area for diffusive gas exchange, and thus significant wave height is a parameter that is particularly important for gases heavily impacted by bubbles. These very large correlation coefficients, especially for H_s with ΔHe and ΔNe (Table 1), show the tight connection between H_s, bubbles, and gas transfer and suggest more work should be done by including H_s in gas exchange parameterizations.

Steady state saturation anomalies of He and Xe are also plotted versus bubble volume and wind wave Reynolds number, Re_{Hw} (Figures 4c–4f), which has been proposed as an alternative to wind speed for use in gas transfer parameterizations (Brumer et al., 2017). For all these variables, there is a general trend for increasing steady state saturation anomalies as the variable increases, but like for wind speed, there is usually a flattening of the gas response at high values. Correlation coefficients between the steady state saturation anomalies and these parameters (Table 1) suggest that when considering all the experiments (monochromatic and JONSWAP waves at all temperatures, with water temperature and wave state as categorical predictor variables), the strongest correlations are with bubble volume for the less soluble gases, and with Re_{Hw} (Ar), U_{10} (Kr), and H_s (Xe) for the more soluble gases. When just monochromatic waves at 26°C are used in the correlation analysis, the correlations are stronger between the gases and Re_{Hw} than when all the experimental data were considered. Bubble volume is also important for explaining variation in the less soluble gases (He and Ne) in the monochromatic waves at 26°C.

Greater predictive power is possible when multiple variables are used in the regression analysis. In particular, multilinear regressions with data from all the experiments (once again with water temperature and wave type

Table 1
Adjusted Correlation Coefficients (R^2) From the Multilinear Regressions for the Correlations Between the Steady State Saturation Anomalies of the Gases (Response Variable) and the Environmental Variables Listed (Predictor Variables)

	Bubble volume	Bubble surface area	H_s	Wave steepness	Re_{Hw}	U_{10}
I. All experiments except those where temperature was intentionally manipulated prior to the start of the experiment to produce a disequilibrium						
ΔHe	0.65	0.61	0.43	0.45	0.51	0.58
ΔNe	0.67	0.59	0.45	0.45	0.51	0.59
ΔAr	0.54	0.51	0.55	0.56	0.57	0.66
ΔKr	--	--	0.45	--	0.45	0.49
ΔXe	--	--	0.33	0.32	0.31	0.32
II. Experiments with monochromatic waves and water temperature 26 C						
ΔHe	0.73	--	--	--	0.64	0.67
ΔNe	0.80	--	--	--	0.79	0.72
ΔAr	0.74	--	0.71	--	0.85	0.65
ΔKr	--	--	0.66	--	0.66	--
ΔXe	--	--	--	--	--	--
III. Experiments with JONSWAP waves and water temperature 26 C						
ΔHe	--	0.93	0.95	0.84	0.94	0.92
ΔNe	--	0.90	0.97	0.85	0.96	0.93
ΔAr	--	0.61	0.90	0.87	0.80	0.88
ΔKr	--	--	0.63	0.58	0.50	0.56
ΔXe	--	--	0.52	0.47	--	0.50

Note. Only correlations with $P < 0.05$ are listed. In the first section, where all experiments were included, additional predictor variables in the correlation analysis included water temperature and wave type.

as categorical predictor variables) had the strongest adjusted correlation coefficients for He, Ne, and Ar when predictor variables were Re_{Hw} and bubble volume (Table 2). With those predictor variables, the adjusted correlation coefficient for He, Ne, and Ar were each greater than 0.80. However, for Kr and Xe, including bubble volume did not increase the correlation coefficient. Instead, the strongest multilinear correlations for Kr were those which included Re_{Hw} and U_{10} as predictor variables and for Xe were those which included Re_{Hw} and wave steepness (and water temperature and wave type for both). Wave properties are therefore the most important for explaining the saturation anomalies of the heavier noble gases and bubble properties are most important for explaining the saturation anomalies of the lighter ones.

Table 2
Adjusted Correlation Coefficients (R^2) From the Multilinear Regressions for the Correlations Between the Steady State Saturation Anomalies of the Gases (Response Variable) and the Environmental Variable Listed in Each Column Listed (as a Predictor Variable) With the Additional Predictor Variable of Wave Reynolds Number Being Included in All Cases

	Nothing additional	Bubble volume	Bubble surface area	H_s	Wave steepness	U_{10}
All experiments except those where temperature was intentionally manipulated prior to the start of the experiment to produce a disequilibrium						
ΔHe	0.51	0.85	0.88	0.64	0.54	0.70
ΔNe	0.51	0.90	0.91	0.69	0.52	0.73
ΔAr	0.57	0.81	0.75	0.69	0.61	0.75
ΔKr	0.45	--	--	0.44	0.49	0.52
ΔXe	0.31	--	--	--	0.48	0.38

Note. Water temperature and wave type are also used as categorical predictor variables. Only correlations with $P < 0.05$ are listed. The "nothing additional" has only the wave Reynolds number as the predictor variable.

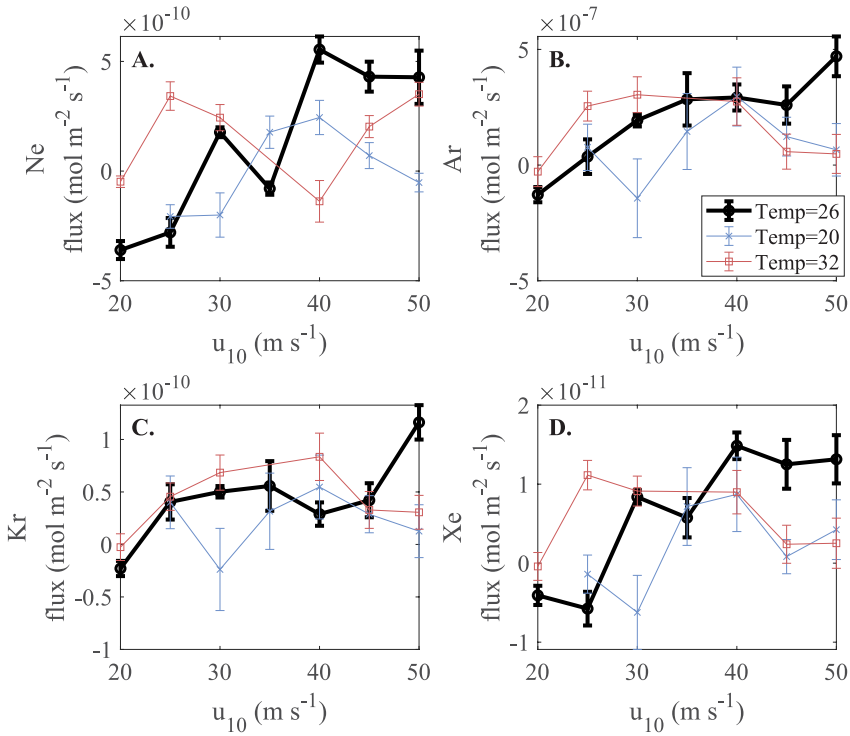

Figure 5. Fluxes of Ne, Ar, Kr, and Xe as a function of wind speed for the experiments with monochromatic waves at three different temperatures (black = 26°C, red = 32°C, and blue = 20°C). Error bars represent the uncertainty in the calculated flux due to the curve fitting of the gas concentrations versus time (see text for details). Note in most cases, flux generally increases as wind speed increases initially but then levels off or even decreases as wind speed continues to increase.

If only the experiments with JONSWAP waves were used in the analysis, then the strongest correlations were when the predictor variable was the significant wave height (Table 1). Adding any of the other possible predictor variables did not improve the correlation coefficient significantly except when initial monochromatic steepness and H_s were used to explain the variance in Xe; the correlation coefficient for Xe increased to 0.77 with predictor variables H_s and wave steepness compared to 0.52 if only H_s was used. This suggests once again the potential of significant wave height, combined with other wave parameters, as an important parameter in gas exchange parameterizations.

3.2. Noble Gas Fluxes

The fluxes of the noble gases in the experiments have larger uncertainties than the steady-state saturation anomalies because the portable mass spectrometer used to measure gas ratios continuously during the experiments is much less precise than the laboratory-based mass spectrometer used to measure discrete samples. Nonetheless, the fluxes of Ne, Ar, Kr, and Xe in the monochromatic wind conditions all show similar qualitative patterns to the steady state saturation anomalies, that is, an initial increase as wind speed increases and then a leveling, or sometimes even a decrease, at very high wind speeds (Figure 5). This behavior is similar to that of aerodynamic drag coefficient (C_d) and suggest a connection between noble gas flux and sea surface roughness. As in the case with the steady state saturation anomalies, the plateau occurs at different wind speeds for different gases and conditions. There is not a significantly different behavior of fluxes as a function of wind speed for the three water temperatures, suggesting that neither water viscosity nor the difference in temperature between atmosphere and water were dominant factors for the gas fluxes. The fluxes for the noble gases in the JONSWAP wave conditions were very low, likely because of the decreased wave-breaking (Smith et al., 2022) in those conditions, and did not appear to change much from experiment to experiment.

Correlation analysis showed many fewer significant correlations between fluxes and environmental variables than for the steady state saturation anomalies (Table 3). This may be because of the larger uncertainties in the

Table 3
Adjusted Correlation Coefficients (R^2) From the Multilinear Regressions for the Correlations Between the Fluxes of the Gases (Response Variable) and the Environmental Variables Listed (Predictor Variable) for the Case With Monochromatic Waves and Water Temperature of 26°C

	Bubble volume	Bubble surface area	H_s	Wave steepness	Re_{Hw}	U_{10}
Experiments with monochromatic waves and water temperature of 26°C						
Ne Flux	0.82	--	--	0.80	0.77	0.79
Ar Flux	0.83	0.57	0.67	0.81	0.91	0.82
Kr Flux	--	--	--	0.69	0.58	0.58
Xe Flux	0.82	--	0.65	0.77	0.87	0.76

Note. Only correlations with $P < 0.05$ are listed.

flux calculations obscuring relationships or may be because fluxes incorporate both the timing of the change as well as the difference in saturation and thus may have a more complicated dependence on physical parameters. Only fluxes in the case of monochromatic waves, 26°C water temperature showed significant correlations. For those experiments, the strongest correlations occurred when the predictor variable was either the bubble volume, the wave steepness, or Re_{Hw} (Table 3). Wind speed also had strong correlations, with an adjusted R^2 of greater than 0.76 for fluxes of all gases except for Kr. Interestingly, H_s was not a strong predictor of flux, perhaps because in monochromatic experiments, the significant wave height remained in a very narrow range, as prescribed by the wave paddles. The JONSWAP experiments, which in the cases of steady state saturation anomalies showed a strong correspondence with H_s, had fluxes with too large uncertainties to show significant correlations to any environmental variables. In summary, the noble gas fluxes, while of more limited use than the saturation anomalies due to the larger measurement uncertainties, also showed a leveling off at more energetic conditions. In one set of experiments, significant correlations were found with a number of typical (i.e., U_{10}) and not so typical (wave steepness, Re_{Hw}, and bubble volume) variables used in gas exchange parameterizations.

Noble gas fluxes as calculated in this study are compared to fluxes predicted by several proposed empirical-based models, namely those of Stanley, Jenkins, et al. (2009), (S09), Liang et al. (2013), (L13), and data from Nicholson et al. (2016), (N16), as parameterized in Emerson et al. (2019). These empirical parameterizations all estimate bubble fluxes (due to both small bubbles that completely dissolve and larger bubbles that partially dissolve) and diffusive gas exchange fluxes based on wind speed only—they do not use bubble spectra or wave data. They were derived using data from the open ocean (the BATS site in S09, Weddell Sea in N16), or were based on detailed bubble models (L13). None of the parameterizations were developed using data at high wind speeds. All three parametrizations predict that gas fluxes will increase as wind speeds increase (Figure 6) but the data in this study show that fluxes level off even as wind speed increases. Note also that these three parameterizations vastly overestimate the flux at high wind speeds ($U_{10} > 30$ m s^{-1}). Some of this discrepancy is due to the difference in wind dependence; a flux that is predicted to increase as the square or cube of the wind speed will certainly be larger than one that does not change as wind speed increases beyond a certain threshold. But also, some of this difference is likely due to the very different nature of these flux estimates. S09, L13, and N16 are all based on expectations for the open ocean. These data were collected in a wind-wave tank. Limitations in a wind-wave tank, especially the shallow depth but also the limited fetch, make it unlikely that fluxes in a wind-wave tank will be identical to those in the ocean. Thus, perhaps the most use of this data will come from combining the wealth of concurrent data from this study on noble gas fluxes, detailed bubble spectra, and wave parameters with mechanistic models that are based on underlying physics of air-sea gas exchange (e.g., Deike & Melville, 2018; Deike et al., 2017; Jeffery et al., 2010; Liang et al., 2017; Reichl & Deike, 2020; Woolf et al., 2007). Though beyond the scope of this paper, the data presented here could be used to help constrain parameters and processes in such mechanistic models, which will in turn allow the mechanistic models to be able to do a better job at quantifying air-sea gas exchange fluxes.

3.3. Invasion Versus Evasion

Fluxes of the noble gases in experiments where deliberate net invasion (e.g., net gas flux into the water) occurred versus fluxes where deliberate net evasion (e.g., net gas flux out of water) was dominant were compared to see if there were systemic differences in invasion versus evasion. Such asymmetry has been predicted for decades (Keeling, 1993; Woolf & Thorpe, 1991) but is unaccounted for in many commonly used gas exchange parameterizations (such as all those which do not explicitly include bubbles). While air injection via completely dissolved bubbles will always lead to a flux into the water (invasion), if the gas becomes highly supersaturated, the diffusive gas exchange flux will be out of the water and thus net evasion can occur. We were able to force the system to net invasion or net evasion by causing an undersaturation in the gases prior to starting the winds (for invasion) or a supersaturation in the gases (for evasion). Such manipulation was performed by changing the temperature of the water prior to the experiment since gas solubility increases as water temperature decreases. The measured

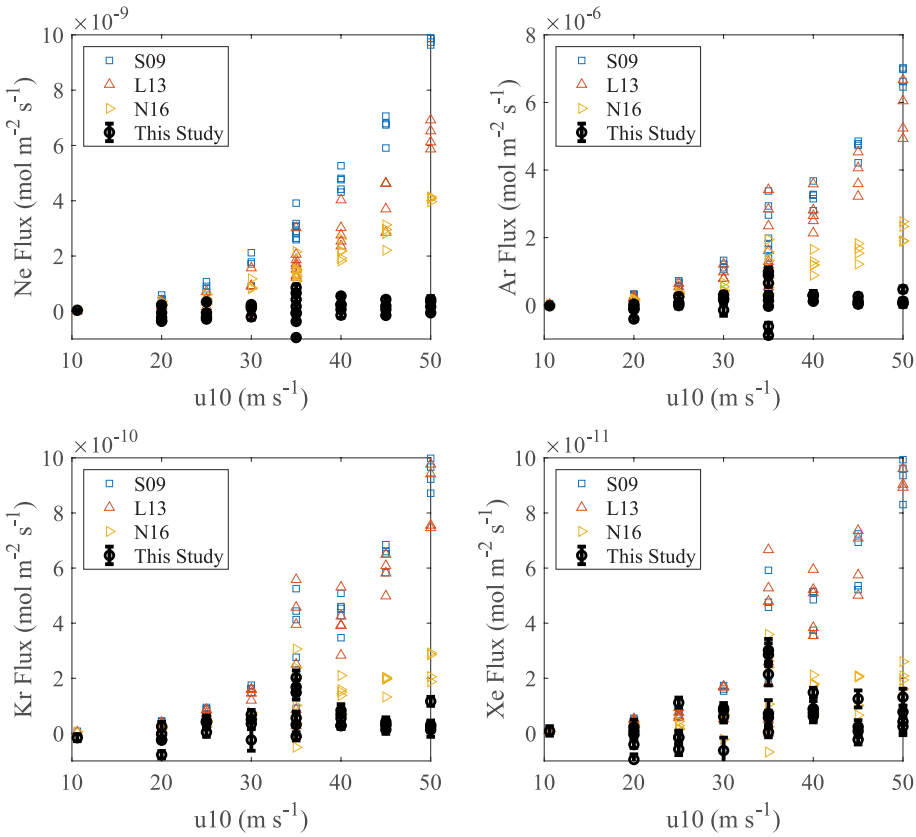

Figure 6. Fluxes of Ne, Ar, Kr, and Xe as a function of wind speed as calculated in this study (black circles, error bars typically are the size of the signal) and as calculated by several gas exchange parameterizations that explicitly include bubbles, namely Stanley, Jenkins, et al., 2009 (S09), Liang et al., 2013 (L13), and Nicholson et al., 2016 (N16). Note the multiple values of the fluxes from both the data and parameterization at different wind speeds are a result of different water temperatures during the experiments. Furthermore, the additional scatter in the data at $U_{10} = 35$ m s^{-1} is because the data reflects experiments with purposeful invasion and evasion as well as the natural flux experiments.

saturation anomalies of the noble gases prior to each deliberate invasion or evasion experiment are listed in Table S2 of Supporting Information S1 and ranged from −5 to −16% for the invasion experiments and to +5 to 8% for the evasion experiments. The concentration data for the net invasion and net evasion experiments that are used to calculate fluxes are shown in Figure S2 of Supporting Information S1.

In particular, in one experiment, the water was first cooled from 32 to 26°C with little gas exchange, creating an undersaturation of gases, whereas in another experiment, the water was warmed from 20 to 26°C, creating a supersaturation of gases. In both cases, winds with $U_{10} = 35$ m/s and monochromatic waves were started and fluxes of the gases were measured. Thus, the wind, wave, and temperature conditions of both experiments were identical except that in one case, the gases started supersaturated whereas in the second case, the gases started undersaturated. The absolute values of the fluxes of all the noble gases were significantly higher in the invasion experiments than the evasion ones (Figure 7). This is likely because in invasion experiments, bubbles and diffusive flux are both bringing gas into the ocean (i.e., working in the same direction). In contrast, in the evasion experiments, bubbles are bringing gas into the ocean but the diffusive flux is forcing gas out of the ocean. Additionally, the Ne concentration in the invasion and evasion experiments was still different after the first 20 min, though ultimately, after about 40 min, the final Ne concentration was the same (Figure S2 of Supporting Information S1).

Evasion and invasion experiments were carried out at other temperatures and conditions as well. Experiments showed that the absolute value of the gas flux was dependent on water temperature with larger fluxes occurring at warmer temperatures—the evasion flux at 32°C was larger than the evasion flux at 26°C, likely because higher water temperatures lead to higher diffusivity rates of the gases and thus larger fluxes or perhaps because of the

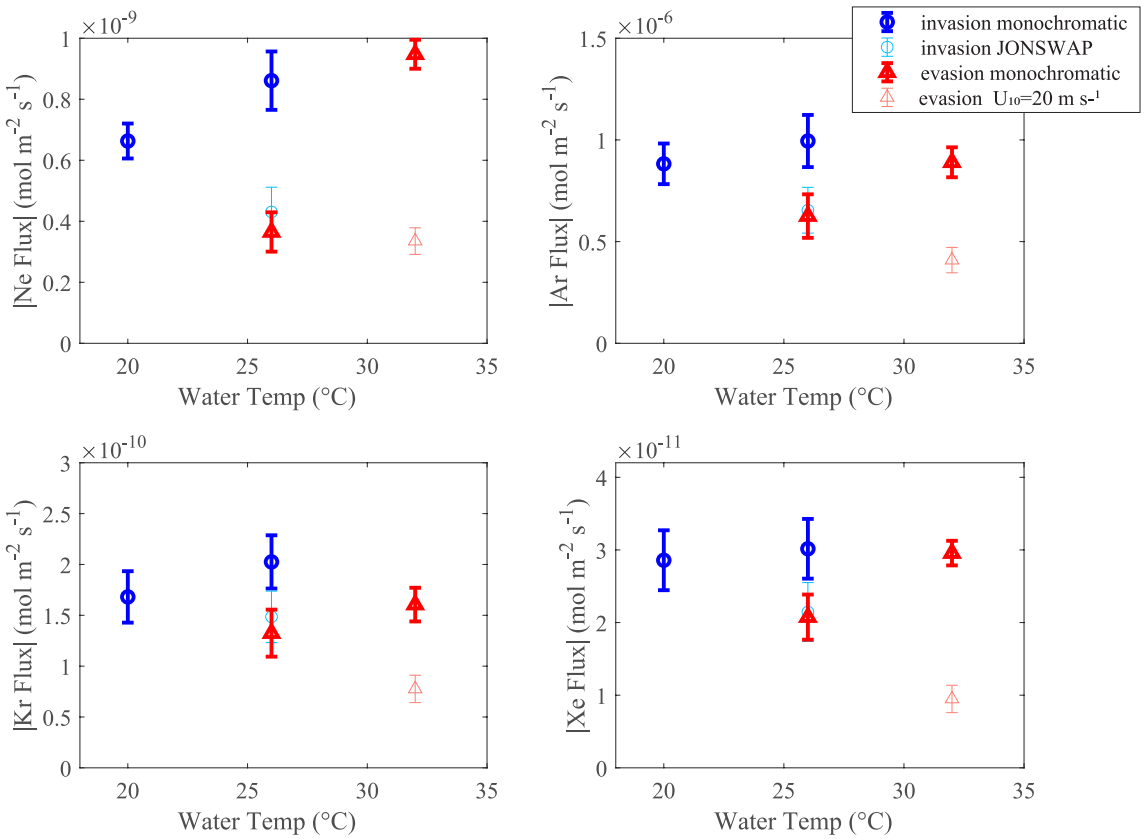

Figure 7. Absolute value of fluxes of Ne, Ar, Kr, and Xe in invasion experiments (blue) and evasion experiments (red) plotted as a function of the water temperature at the time of the experiment. In the invasion experiments, the water was cooled 6°C with little gas exchange prior to beginning the experiment leading to an undersaturation of the gases; in the evasion experiments, the water was warmed 6°C prior to the beginning of the experiment, leading to initial supersaturations. Wind speeds were $U_{10} = 35$ m s^{-1} for the bold symbols. For the pale blue experiment, $U_{10} = 35$ m s^{-1} but the wave type was JONSWAP. For the pale red experiment, the wave type was monochromatic but $U_{10} = 20$ m s^{-1}.

smaller solubility of the gases at the higher water temperatures. One invasion experiment was performed with JONSWAP waves rather than monochromatic waves. The JONSWAP experiment had significantly lower fluxes of all the gases, likely because the JONSWAP experiments had much less wave breaking, as shown by it having approximately half the bubble volume and a smaller wave steepness (Smith et al., 2022). The differences between the JONSWAP and the monochromatic wave experiments were greatest for the Ne fluxes, the gas that is most influenced by bubbles.

In summary, the differences in invasion fluxes compared to evasion fluxes means that when using a gas exchange parameterization, it is important to consider if that parameterization was derived during conditions of invasion or evasion and/or if the parameterization explicitly accounts for bubble injection. For example, the dual tracer release method is based on evasion, whereas eddy correlation studies are sometimes based on invasion and sometimes on evasion (depending on the gas and location being studied). Explicitly accounting for bubble fluxes when calculating gas exchange from parameterizations is likely to lessen any effects of interchanging evasion versus invasion-derived parameterizations.

Additionally, the differences in invasion versus evasion fluxes for the same conditions could explain why this study (which was primarily invasion) shows a flattening of the gas fluxes and steady state saturation anomalies as wind speed increases, whereas work by Krall et al. (2019), which was all based on evasion in a wind-wave tank, shows a continued increase in flux as wind speed increases. Most experiments in this study were based on invasion because gas saturation state was brought close to 0 at the beginning of each experiment by the gentle winds and mixing and then when the experiments started, bubble fluxes caused the noble gases in the atmosphere to invade into the water. This occurred because the water was not manipulated (i.e., no gases artificially added) prior to the experiments and noble gases are present in the atmosphere. As bubbles entered the water, the water

became supersaturated and thus evasion occurred due to diffusive gas exchange. Thus, steady states were reached where these two opposing forces worked against each other. As wind speeds increases, fluxes plateaued because both the inward bubbles and the outward diffusive gas exchange got stronger, even as wind speed increased.

In contrast, in the experiments by Krall et al. (2019) the mechanism of gas transfer was evasion. This is because prior to all those experiments, gases were injected into the water in the tank through the use of membrane contactors and gas tanks (Krall et al., 2019). Many of the gases used in that experiment have extremely low concentrations in air (e.g., SF_6, PFE, C_2H_2, HFB, CH_2F_2, and MA) and thus there was no physical way for atmospheric air to enter the water through invasion due to natural bubbles. Hence, the Krall et al. (2019) experiments were solely evasion and there was no balancing of inward and outward fluxes. Hence the gas transfer could increase as wind speed increased with no flattening. Note that the only role bubbles could play in those experiments was to aid evasion—if gases are highly supersaturated, gases can diffuse into the bubbles and be carried out of the water with the bubbles acting as another interface for exchange and resulting in an additional evasion flux.

4. Conclusions

Gas exchange at high wind speeds is a crucial unknown given the lack of data collected at wind speeds greater than $U_{10} = 25$ m s^{-1} and the large extent to which existing gas exchange parameterizations diverge at high wind speeds. This study investigated gas exchange in a wind-wave tank which enabled investigation of gas fluxes and steady state saturation anomalies at wind speeds up to 50 m s^{-1}. We found that both steady state saturation anomalies and fluxes increased initially and then leveled off at high wind speeds. This in part may be because the bubble radii shifted to smaller radii at very high wind speeds and the total void fraction due to bubbles flattened as wind speed continued to increase above ~35 m s^{-1} (Smith et al., 2022). Previous work has shown that heat and momentum flux coefficients level off at approximately $U_{10} = 30$–35 m s^{-1} (Donelan et al., 2004; Haus et al., 2010; Jarosz et al., 2007; Takagaki et al., 2016) though some studies suggest it may be only momentum flux coefficient that levels off and that heat fluxes continue to increase as wind speed increases (Komori et al., 2018). Field observations support the leveling off of heat and momentum flux coefficients at high wind speeds (Bell et al., 2012; Jarosz et al., 2007; Powell et al., 2003). The mechanism for this flattening is not known but may be related to flow separation at very high wind speeds, shear instabilities, and/or saturation of energy at the air-sea interface. In this study, experiments were conducted with two types of wave conditions and at three temperatures and the same general flattening of gas flux and steady state saturation anomalies was found in all conditions though the exact wind speed at which the flattening occurred differed in the various environmental conditions.

A second important finding of this work was that wave statistics (such as H_s and wave steepness) do a better job at predicting gas fluxes than wind speed in the JONSWAP wave conditions (the wave condition most similar to the real ocean). It is possible to obtain estimates of wave statistics from modeling (Romero, 2019) so wave statistics could be used widely in gas exchange parameterizations (Deike & Melville, 2018; Reichil & Deike, 2020), either directly or through the wave wind Reynolds number, Re_{Hw} (Brumer et al., 2017). Bubble volume and surface area were also important variables that could explain a large fraction of the variance for the least soluble gases (He, Ne, and Ar). Future work includes developing and then constraining a bubble model with the noble gases and shadowgraph bubble data from this study in order to assess which bubble properties (volume, surface area, radius, etc.) are most useful for predicting gas fluxes and steady state saturation anomalies and the dependencies of gas fluxes on those parameters.

Third, the experimental data showed important differences between invasion and evasion for all the noble gases, even the most soluble ones such as Xe. However, many commonly used gas exchange parameterizations do not distinguish between invasion and evasion. This work shows that such lack of distinction will lead to errors. Using air-sea gas exchange parameterizations that explicitly include bubble fluxes (Blomquist et al., 2017; Fairall et al., 2011; Goddijn-Murphy et al., 2016; Liang et al., 2013; Nicholson et al., 2011; Stanley, Jenkins, et al., 2009; Zhang, 2012) is advisable since then differences between invasion and evasion will be accounted for.

While the wind-wave tank provides an excellent closed system that can be tightly monitored, and that enables very high wind speeds to be experimentally studied, questions remain on how applicable these results are to an open ocean setting. In particular, the water depth in the SUSTAIN tank (0.8 m) is much shallower than the maximum depth of bubble plumes in the ocean, which can extend to 38 m deep (Strand et al., 2020) though mean bubble penetration depth is likely to be within the depth of the SUSTAIN tank (estimated at less than

0.5 m [Callaghan, 2018; Callaghan et al., 2012]). Additionally, although features of the tank such as the sloping beach reduce limitations due to the short fetch in the tank, the tank certainly is not the same as the real ocean. Therefore, this study is missing the flux due to deep bubbles. Nonetheless, given that the vast majority of bubbles only reach shallower depths, the omission of deep bubble plumes may not be very problematic. Additionally, including a deep bubble flux would likely strengthen some of the findings of this paper—there should be even greater differences in invasion versus evasion if all bubbles were included and wave breaking statistics would be even more important for inclusion in parameterizations. However, the flattening of the fluxes and steady state saturation anomalies at very high wind speeds might not occur if deep bubbles were present and could transfer large amounts of gas since deep bubbles provide a mechanism for enhanced bubble injection when shallow bubble injection reaches a maximum. Thus, it is imperative for more field observations of gas fluxes and steady state saturation anomalies in high wind conditions (such as work by Liang et al. [2020] and McNeil and D'Asaro [2007] on measurements collected autonomously in typhoons). Thus, the main power of this study is that it points to intriguing behavior that should be tested in the real ocean (i.e., the flattening of the fluxes and steady state saturation anomalies) as well as key variables (significant wave height, wave steepness, and wave dependent Reynolds number) that should be further studied.

Data Availability Statement

Data on all the parameters measured in the experiment are available at the Biological and Chemical Oceanography Data Management (BCO-DMO) database (https://www.bco-dmo.org/project/776111). In particular, the noble gas discrete data can be found at https://www.bco-dmo.org/dataset/869304 and the continuous noble gas concentration data from the GEMS can be found at https://www.bco-dmo.org/dataset/869295. Global wind speed C-2015 ASCAT data (used for Figure S1 in Supporting Information S1) are produced by Remote Sensing Systems and sponsored by the NASA Ocean Vector Winds Science Team; ASCAT data are available at www.remss.com.

Acknowledgments
This work was supported by the National Science Foundation (Grant OCE1634467 and OCE1634432). We are grateful for the assistance of members of the SUSTAIN lab at the University of Miami for assistance in setting up the experiments and collecting data and to William Jenkins and Dempsey Lott of the WHOI Isotope Geochemistry Facility for noble gas analysis of copper tube samples. We also are grateful for the GitHub gas toolbox of David Nicholson and Cara Man (https://github.com/dnicholson/gas_toolbox) that was used to calculate gas fluxes from the S09, L13, and N16 parameterizations. We thank two anonymous reviewers for their helpful suggestions that improved this manuscript.

References

Alkire, M. B., Lee, C., D'Asaro, E., Perry, M. J., Briggs, N., Cetinic, I., & Gray, A. (2014). Net community production and export from Seaglider measurements in the North Atlantic after the spring bloom. *Journal of Geophysical Research: Oceans*, *119*(9), 6121–6139. https://doi.org/10.1002/2014jc010105

Asher, W. E., Karle, L. M., Higgins, B. J., Farley, P. J., Monahan, E. C., & Leifer, I. S. (1996). The influence of bubble plumes on air-seawater gas transfer velocities. *Journal of Geophysical Research*, *101*(C5), 12027–12041. https://doi.org/10.1029/96jc00121

Atherton, T. J., & Kerbyson, D. J. (1999). Size invariant circle detection. *Image and Vision Computing*, *17*(11), 795–803. https://doi.org/10.1016/s0262-8856(98)00160-7

Babanin, A., Chalikov, D., Young, I., & Savelyev, I. (2007). Predicting the breaking onset of surface water waves. *Geophysical Research Letters*, *34*(7), L07605. https://doi.org/10.1029/2006gl029135

Bell, M. M., Montgomery, M. T., & Emanuel, K. A. (2012). Air-sea enthalpy and momentum exchange at major hurricane wind speeds observed during CBLAST. *Journal of the Atmospheric Sciences*, *69*(11), 3197–3222. https://doi.org/10.1175/jas-d-11-0276.1

Bell, T. G., Landwehr, S., Miller, S. D., de Bruyn, W. J., Callaghan, A. H., Scanlon, B., et al. (2017). Estimation of bubble-mediated air–sea gas exchange from concurrent DMS and CO_2 transfer velocities at intermediate–high wind speeds. *Atmospheric Chemistry and Physics*, *17*(14), 9019–9033. https://doi.org/10.5194/acp-17-9019-2017

Blomquist, B. W., Brumer, S. E., Fairall, C. W., Huebert, B. J., Zappa, C. J., Brooks, I. M., et al. (2017). Wind speed and sea state dependencies of air-sea gas transfer: Results from the high wind speed gas exchange study (HiWinGS). *Journal of Geophysical Research: Oceans*, *122*(10), 8034–8062. https://doi.org/10.1002/2017jc013181

Blomquist, B. W., Fairall, C. W., Huebert, B. J., & Wilson, S. T. (2012). Direct measurement of the oceanic carbon monoxide flux by eddy correlation. *Atmospheric Measurement Techniques*, *5*(12), 3069–3075. https://doi.org/10.5194/amt-5-3069-2012

Brumer, S. E., Zappa, C. J., Blomquist, B. W., Fairall, C. W., Cifuentes-Lorenzen, A., Edson, J. B., et al. (2017). Wave-related Reynolds number parameterizations of CO_2 and DMS transfer velocities. *Geophysical Research Letters*, *44*(19), 9865–9875. https://doi.org/10.1002/2017gl074979

Callaghan, A. H. (2018). On the relationship between the energy dissipation rate of surface-breaking waves and oceanic whitecap coverage. *Journal of Physical Oceanography*, *48*(11), 2609–2626. https://doi.org/10.1175/jpo-d-17-0124.1

Callaghan, A. H., Deane, G. B., Stokes, M. D., & Ward, B. (2012). Observed variation in the decay time of oceanic whitecap foam. *Journal of Geophysical Research*, *117*(C9), C09015. https://doi.org/10.1029/2012jc008147

Cassar, N., Barnett, B. A., Bender, M. L., Kaiser, J., Hamme, R. C., & Tilbrook, B. (2009). Continuous high-frequency dissolved O_2/Ar measurements by equilibrator inlet mass spectrometry. *Analytical Chemistry*, *81*(5), 1855–1864. https://doi.org/10.1021/ac802300u

D'Asaro, E., & McNeil, C. (2007). Air-sea gas exchange at extreme wind speeds measured by autonomous oceanographic floats. *Journal of Marine Systems*, *66*(1–4), 92–109. https://doi.org/10.1016/j.jmarsys.2006.06.007

Deike, L., Lenain, L., & Melville, W. K. (2017). Air entrainment by breaking waves. *Geophysical Research Letters*, *44*(8), 3779–3787. https://doi.org/10.1002/2017gl072883

Deike, L., & Melville, W. K. (2018). Gas transfer by breaking waves. *Geophysical Research Letters*, *45*(19), 10482–10492. https://doi.org/10.1029/2018gl078758

Donelan, M. A., Drennan, W. M., & Magnusson, A. K. (1996). Nonstationary analysis of the directional properties of propagating waves. *Journal of Physical Oceanography*, *26*(9), 1901–1914. https://doi.org/10.1175/1520-0485(1996)026<1901:naotdp>2.0.co;2

Donelan, M. A., Haus, B. K., Reul, N., Plant, W. J., Stiassnie, M., Graber, H. C., et al. (2004). On the limiting aerodynamic roughness of the ocean in very strong winds. *Geophysical Research Letters*, *31*(18), L18306. https://doi.org/10.1029/2004gl019460

Emerson, S. (2014). Annual net community production and the biological carbon flux in the ocean. *Global Biogeochemical Cycles*, *28*(1), 14–28. https://doi.org/10.1002/2013gb004680

Emerson, S., Yang, B., White, M., & Cronin, M. (2019). Air-sea gas transfer: Determining bubble fluxes with in situ N_2 observations. *Journal of Geophysical Research: Oceans*, *124*(4), 2716–2727. https://doi.org/10.1029/2018JC014786

Fairall, C. W., Yang, M. X., Bariteau, L., Edson, J. B., Helmig, D., McGillis, W., et al. (2011). Implementation of the coupled ocean-atmosphere response experiment flux algorithm with CO_2, dimethyl sulfide, and O_3. *Journal of Geophysical Research*, *116*, C00F09. https://doi.org/10.1029/2010jc006884

Goddijn-Murphy, L., Woolf, D. K., Callaghan, A. H., Nightingale, P. D., & Shutler, J. D. (2016). A reconciliation of empirical and mechanistic models of the air-sea gas transfer velocity. *Journal of Geophysical Research: Oceans*, *121*(1), 818–835. https://doi.org/10.1002/2015JC011096

Gu, Y. Y., Katul, G. G., & Cassar, N. (2021). The intensifying role of high wind speeds on air-sea carbon dioxide exchange. *Geophysical Research Letters*, *48*(5), e2020GL090713. https://doi.org/10.1029/2020gl090713

Hamme, R. C., Cassar, N., Lance, V. P., Vaillancourt, R. D., Bender, M. L., Strutton, P. G., et al. (2012). Dissolved O_2/Ar and other methods reveal rapid changes in productivity during a Lagrangian experiment in the Southern Ocean. *Journal of Geophysical Research*, *117*(C4), C00F12. https://doi.org/10.1029/2011JC007046

Hamme, R. C., & Emerson, S. (2004). The solubility of neon, nitrogen and argon in distilled water and seawater. *Deep-Sea Research I*, *51*(11), 1517–1528. https://doi.org/10.1016/j.dsr.2004.06.009

Hamme, R. C., & Emerson, S. (2006). Constraining bubble dynamics and mixing with dissolved gases: Implications for productivity measurements by oxygen mass balance. *Journal of Marine Research*, *64*(1), 73–95. https://doi.org/10.1357/002224006776412322

Hamme, R. C., & Severinghaus, J. P. (2007). Trace gas disequilibria during deep-water formation. *Deep-Sea Research Part I Oceanographic Research Papers*, *54*(6), 939–950. https://doi.org/10.1016/j.dsr.2007.03.008

Hasselman, K., Barnett, T. P., Bouws, E., Carlson, H., Carwright, D. E., Enke, K., et al. (1973). Measurements of wind-wave growth and swell decay during the Joint Norht Sea Wave Project (JONSWAP). *Supplement to the German Hydrographic Journal*, *12*(1), 10–90.

Haus, B. K., Jeong, D., Donelan, M. A., Zhang, J. A., & Savelyev, I. (2010). Relative rates of sea-air heat transfer and frictional drag in very high winds. *Geophysical Research Letters*, *37*(7), L07802. https://doi.org/10.1029/2009gl042206

Ho, D. T., Law, C. S., Smith, M. J., Schlosser, P., Harvey, M., & Hill, P. (2006). Measurements of air-sea gas exchange at high wind speeds in the Southern Ocean: Implications for global parameterizations. *Geophysical Research Letters*, *33*(16), L16611. https://doi.org/10.1029/2006gl026817

Ho, D. T., Wanninkhof, R., Schlosser, P., Ullman, D. S., Hebert, D., & Sullivan, K. F. (2011). Toward a universal relationship between wind speed and gas exchange: Gas transfer velocities measured with $^3He/SF_6$ during the Southern Ocean Gas Exchange Experiment. *Journal of Geophysical Research*, *116*, C00F04. https://doi.org/10.1029/2010jc006854

Huebert, B. J., Blomquist, B. W., Hare, J. E., Fairall, C. W., Johnson, J. E., & Bates, T. S. (2004). Measurement of the sea-air DMS flux and transfer velocity using eddy correlation. *Geophysical Research Letters*, *31*(23). https://doi.org/10.1029/2004GL021567

Jahne, B., Heinz, G., & Dietrich, W. (1987). Measurement of the diffusion coefficients of sparingly soluble gases in water. *Journal of Geophysical Research*, *92*(C10), 10767–10776. https://doi.org/10.1029/jc092ic10p10767

Jarosz, E., Mitchell, D. A., Wang, D. W., & Teague, W. J. (2007). Bottom-up determination of air-sea momentum exchange under a major tropical cyclone. *Science*, *315*(5819), 1707–1709. https://doi.org/10.1126/science.1136466

Jeffery, C. D., Robinson, I. S., & Woolf, D. K. (2010). Tuning a physically-based model of the air-sea gas transfer velocity. *Ocean Modelling*, *31*(1–2), 28–35. https://doi.org/10.1016/j.ocemod.2009.09.001

Jenkins, W. J., Lott, D. E., & Cahill, K. L. (2019). A determination of atmospheric helium, neon, argon, krypton, and xenon solubility concentrations in water and seawater. *Marine Chemistry*, *211*, 94–107. https://doi.org/10.1016/j.marchem.2019.03.007

Johnson, K. S., & Bif, M. B. (2021). Constraint on net primary productivity of the global ocean by Argo oxygen measurements. *Nature Geoscience*, *14*(10), 769–774. https://doi.org/10.1038/s41561-021-00807-z

Juranek, L. W., Quay, P. D., Feely, R. A., Lockwood, D., Karl, D. M., & Church, M. J. (2012). Biological production in the NE Pacific and its influence on air-sea CO_2 flux: Evidence from dissolved oxygen isotopes and O_2/Ar. *Journal of Geophysical Research*, *117*(C5), C05022. https://doi.org/10.1029/2011JC007450

Keeling, R. F. (1993). On the role of large bubbles in air-sea gas-exchange and supersaturation in the ocean. *Journal of Marine Research*, *51*(2), 237–271. https://doi.org/10.1357/0022240933223800

Komori, S., Iwano, K., Takagaki, N., Onishi, R., Kurose, R., Takahashi, K., & Suzuki, N. (2018). Laboratory measurements of heat transfer and drag coefficients at extremely high wind speeds. *Journal of Physical Oceanography*, *48*(4), 959–974. https://doi.org/10.1175/jpo-d-17-0243.1

Krall, K. E., & Jaehne, B. (2014). First laboratory study of air-sea gas exchange at hurricane wind speeds. *Ocean Science*, *10*(2), 257–265. https://doi.org/10.5194/os-10-257-2014

Krall, K. E., Smith, A. W., Takagaki, N., & Jahne, B. (2019). Air-sea gas exchange at wind speeds up to 85 m s^{-1}. *Ocean Science*, *15*(6), 1783–1799. https://doi.org/10.5194/os-15-1783-2019

Laxague, N. J. M., Haus, B. K., Ortiz-Suslow, D. G., Smith, C. J., Novelli, G., Dai, H., et al. (2017). Passive optical sensing of the near-surface wind-driven current profile. *Journal of Atmospheric and Oceanic Technology*, *34*(5), 1097–1111. https://doi.org/10.1175/jtech-d-16-0090.1

Li, S., Babanin, A. V., Qiao, F. L., Dai, D. J., Jiang, S. M., & Guan, C. L. (2021). Laboratory experiments on CO_2 gas exchange with wave breaking. *Journal of Physical Oceanography*, *51*(10), 3105–3116. https://doi.org/10.1175/jpo-d-20-0272.1

Liang, J. H., D'Asaro, E. A., McNeil, C. L., Fan, Y. L., Harcourt, R. R., Emerson, S. R., et al. (2020). Suppression of CO_2 outgassing by gas bubbles under a hurricane. *Geophysical Research Letters*, *47*(18), e2020GL090249. https://doi.org/10.1029/2020gl090249

Liang, J. H., Deutsch, C., McWilliams, J. C., Baschek, B., Sullivan, P. P., & Chiba, D. (2013). Parameterizing bubble-mediated air-sea gas exchange and its effect on ocean ventilation. *Global Biogeochemical Cycles*, *27*(3), 894–905. https://doi.org/10.1002/gbc.20080

Liang, J. H., Emerson, S. R., D'Asaro, E. A., McNeil, C. L., Harcourt, R. R., Sullivan, P. P., et al. (2017). On the role of sea-state in bubble-mediated air-sea gas flux during a winter storm. *Journal of Geophysical Research: Oceans*, *122*(4), 2671–2685. https://doi.org/10.1002/2016JC012408

Liang, J. H., McWilliams, J. C., Sullivan, P. P., & Baschek, B. (2011). Modeling bubbles and dissolved gases in the ocean. *Journal of Geophysical Research*, *116*(C3), C03015. https://doi.org/10.1029/2010jc006579

Loose, B., Jenkins, W. J., Moriarty, R., Brown, P., Jullion, L., Garabato, A. C. N., et al. (2016). Estimating the recharge properties of the deep ocean using noble gases and helium isotopes. *Journal of Geophysical Research: Oceans*, *121*(8), 5959–5979. https://doi.org/10.1002/2016jc011809

Manning, C., Stanley, R. H. R., & Lott, III, D. E. (2016). Continuous measurements of dissolved Ne, Ar, Kr, and Xe ratios with a field-deployable gas equilibration mass spectrometer. *Analytical Chemistry*, *88*(6), 3040–3048. https://doi.org/10.1021/acs.analchem.5b03102

McGillis, W. R., Edson, J. B., Zappa, C. J., Ware, J. D., McKenna, S. P., Terray, E. A., et al. (2004). Air-sea CO_2 exchange in the equatorial Pacific. *Journal of Geophysical Research*, *109*(C8), C08S02. https://doi.org/10.1029/2003jc002256

McNeil, C., & D'Asaro, E. (2007). Parameterization of air-sea gas fluxes at extreme wind speeds. *Journal of Marine Systems*, *66*(1–4), 110–121. https://doi.org/10.1016/j.jmarsys.2006.05.013

Mesarchaki, E., Kraeuter, C., Krall, K. E., Bopp, M., Helleis, F., Williams, J., & Jaehne, B. (2015). Measuring air-sea gas-exchange velocities in a large-scale annular wind-wave tank. *Ocean Science*, *11*(1), 121–138. https://doi.org/10.5194/os-11-121-2015

Nicholson, D., Emerson, S., & Khatiwala, S. (Eds.). (2011). *An inverse approach to estimate bubble-mediated air-sea gas flux from inert gas measurements*. Kyoto University Press.

Nicholson, D. P., Khatiwala, S., & Heimbach, P. (2016). Noble gas tracers of ventilation during deep-water formation in the Weddell Sea. *IOP Conference Series: Earth and Environmental Science*, *35*(1), 012019. https://doi.org/10.1088/1755-1315/35/1/012019

Nicholson, D. P., Wilson, S. T., Doney, S. C., & Karl, D. M. (2015). Quantifying subtropical North Pacific gyre mixed layer primary productivity from Seaglider observations of diel oxygen cycles. *Geophysical Research Letters*, *42*(10), 4032–4039. https://doi.org/10.1002/2015gl063065

Nightingale, P. D., Malin, G., Law, C. S., Watson, A., Liss, P. S., Liddicoat, M. I., et al. (2000). In situ evaluation of air-sea gas exchange parameterizations using novel conservative and volatile tracers. *Global Biogeochemical Cycles*, *14*(1), 373–387. https://doi.org/10.1029/1999gb900091

Ozgokmen, T. M., Boufadel, M., Carlson, D. F., Cousin, C., Guigand, C., Haus, B. K., et al. (2018). Technological advances for ocean surface measurements by the consortium for advanced research on transport of hydrocarbons in the environment (CARTHE). *Marine Technology Society Journal*, *52*(6), 71–76. https://doi.org/10.4031/mtsj.52.6.11

Palevsky, H. I., Quay, P. D., Lockwood, D. E., & Nicholson, D. P. (2016). The annual cycle of gross primary product ion, net community production, and export efficiency across the North Pacific Ocean. *Global Biogeochemical Cycles*, *30*(2), 361–380. https://doi.org/10.1002/2015GB005318

Plant, J. N., Johnson, K. S., Sakamoto, C. M., Jannasch, H. W., Coletti, L. J., Riser, S. C., & Swift, D. D. (2016). Net community production at Ocean Station Papa observed with nitrate and oxygen sensors on profiling floats. *Global Biogeochemical Cycles*, *30*(6), 859–879. https://doi.org/10.1002/2015GB005349

Powell, M. D., Vickery, P. J., & Reinhold, T. A. (2003). Reduced drag coefficient for high wind speeds in tropical cyclones. *Nature*, *422*(6929), 279–283. https://doi.org/10.1038/nature01481

Reichil, B. G., & Deike, L. (2020). Contribution of sea-state dependent bubbles to air-sea carbon dioxide fluxes. *Geophysical Research Letters*, *47*(9), e2020GL087267. https://doi.org/10.1029/2020gl087267

Ricciardulli, L., & Wentz, F. J. (2016). In C. R. S. S. Santa Rosa (Ed.), *Remote Sensing Systems ASCAT C-2015 Daily Ocean Vector Winds on 0.25 deg grid, Version 02.1*. Retrieved from www.remss.com

Romero, L. (2019). Distribution of surface wave breaking fronts. *Geophysical Research Letters*, *46*(17–18), 10463–10474. https://doi.org/10.1029/2019gl083408

Savelyev, I. B., Buckley, M. P., & Haus, B. K. (2020). The impact of nonbreaking waves on wind-driven ocean surface turbulence. *Journal of Geophysical Research: Oceans*, *125*(1), e2019JC015573. https://doi.org/10.1029/2019jc015573

Smith, A. W., Haus, B. K., & Stanley, R. H. R. (2022). Bubble-turbulence dynamics and dissipation beneath laboratory breaking and non-breaking waves. *Journal of Physical Oceanography*, *52*(9), 2159–2181. in press. https://doi.org/10.1175/JPO-D-21-0209.1

Spitzer, W. S., & Jenkins, W. J. (1989). Rates of vertical mixing, gas-exchange and new production - Estimates from seasonal gas cycles in the upper ocean near Bermuda. *Journal of Marine Research*, *47*(1), 169–196. https://doi.org/10.1357/002224089785076370

Stanley, R. H. R., Baschek, B., Lott, D. E., & Jenkins, W. J. (2009). A new automated method for measuring noble gases and their isotopic ratios in water samples. *Geochemistry, Geophysics, Geosystems*, *10*(5), Q05008. https://doi.org/10.1029/2009GC002429

Stanley, R. H. R., Jenkins, W. J., & Doney, S. C. (2006). Quantifying seasonal air-sea gas exchange processes using noble gas time-series: A design experiment. *Journal of Marine Research*, *64*(2), 267–295. https://doi.org/10.1357/002224006777606452

Stanley, R. H. R., Jenkins, W. J., Doney, S. C., & Lott, III, D. E. (2009). Noble gas constraints on air-sea gas exchange and bubble fluxes. *Journal of Geophysical Research*, *114*(C11), C11020. https://doi.org/10.1029/2009JC005396

Stanley, R. H. R., Sandwith, Z. O., & Williams, W. J. (2015). Rates of summertime biological productivity in the Beaufort Gyre: A comparison between the low and record-low ice conditions of August 2011 and 2012. *Journal of Marine Systems*, *147*, 29–44. https://doi.org/10.1016/j.jmarsys.2014.04.006

Strand, K. O., Breivik, O., Pedersen, G., Vikebo, F. B., Sundby, S., & Christensen, K. H. (2020). Long-term statistics of observed bubble depth versus modeled wave dissipation. *Journal of Geophysical Research: Oceans*, *125*(2), e2019JC015906. https://doi.org/10.1029/2019jc015906

Sweeney, C., Gloor, E., Jacobson, A. R., Key, R. M., McKinley, G., Sarmiento, J. L., & Wanninkhof, R. (2007). Constraining global air-sea gas exchange for CO_2 with recent bomb ^{14}C measurements. *Global Biogeochemical Cycles*, *21*(2), GB2015. https://doi.org/10.1029/2006gb002784

Takagaki, N., Komori, S., & Suzuki, N. (2016). Estimation of friction velocity from the wind-wave spectrum at extremely high wind speeds. *IOP Conference Series: Earth and Environmental Sciences*, *35*, 012009. https://doi.org/10.1088/1755-1315/35/1/012009

Vagle, S., McNeil, C., & Steiner, N. (2010). Upper ocean bubble measurements from the NE Pacific and estimates of their role in air-sea gas transfer of the weakly soluble gases nitrogen and oxygen. *Journal of Geophysical Research*, *115*(C12), C12054. https://doi.org/10.1029/2009jc005990

Wanninkhof, R. (1992). Relationship between wind speed and gas exchange over the ocean. *Journal of Geophysical Research*, *97*(C5), 7373–7382. https://doi.org/10.1029/92jc00188

Wanninkhof, R. (2014). Relationship between wind speed and gas exchange over the ocean revisited. *Limnology and Oceanography: Methods*, *12*(6), 351–362. https://doi.org/10.4319/lom.2014.12.351

Wanninkhof, R., Asher, W. E., Ho, D. T., Sweeney, C., & McGillis, W. R. (2009). Advances in quantifying air-sea gas exchange and environmental forcing. *Annual Review of Marine Science*, *1*, 213–244. https://doi.org/10.1146/annurev.marine.010908.163742

Woolf, D. K., Leifer, I. S., Nightingale, P. D., Rhee, T. S., Bowyer, P., Caulliez, G., et al. (2007). Modelling of bubble-mediated gas transfer: Fundamental principles and a laboratory test. *Journal of Marine Systems*, *66*(1–4), 71–91. https://doi.org/10.1016/j.jmarsys.2006.02.011

Woolf, D. K., & Thorpe, S. A. (1991). Bubbles and the air-sea exchange of gases in near-saturation conditions. *Journal of Marine Research*, *49*(3), 435–466. https://doi.org/10.1357/002224091784995765

Wrobel, I., & Piskozub, J. (2016). Effect of gas-transfer velocity parameterization choice on air–sea CO_2 fluxes in the North Atlantic Ocean and the European Arctic. *Ocean Science*, *12*(5), 1091–1103. https://doi.org/10.5194/os-12-1091-2016

Young, C., & Lupton, J. E. (1983). An ultratight fluid sampling system using cold-welded copper tubing. *Eos Transactions AGU*, *64*, 735.

Young, I. R., & Ribal, A. (2019). Multiplatform evaluation of global trends in wind speed and wave height. *Science*, *364*(6440), 548–552. https://doi.org/10.1126/science.aav9527

Young, I. R., Zieger, S., & Babanin, A. V. (2011). Global trends in wind speed and wave height. *Science*, *332*(6028), 451–455. https://doi.org/10.1126/science.1197219

Zappa, C. J., McGillis, W. R., Raymond, P. A., Edson, J. B., Hintsa, E. J., Zemmelink, H. J., et al. (2007). Environmental turbulent mixing controls on air-water gas exchange in marine and aquatic systems. *Geophysical Research Letters*, *34*(10), L10601. https://doi.org/10.1029/2006GL028790

Zavarsky, A., Goddijn-Murphy, L., Steinhoff, T., & Marandino, C. A. (2018). Bubble-mediated gas transfer and gas transfer suppression of DMS and CO_2. *Journal of Geophysical Research: Atmospheres*, *123*(12), 6624–6647. https://doi.org/10.1029/2017jd028071

Zhang, X. (2012). Contribution to the global air-sea CO_2 exchange budget from asymmetric bubble-mediated gas transfer. *Tellus Series B: Chemical and Physical Meteorology*, *64*(1), 17260. https://doi.org/10.3402/tellusb.v64i0.17260